Protein-Enabled Synthesis of Monodisperse Titania Nanoparticles On and Within Polyelectrolyte Matrices

By *Eugenia Kharlampieva, Joseph M. Slocik, Srikanth Singamaneni, Nicole Poulsen, Nils Kröger, Rajesh R. Naik,* and *Vladimir V. Tsukruk**

Here, the results of a study of the mechanism of bio-enabled surface-mediated titania nanoparticle synthesis with assistance of polyelectrolyte surfaces are reported. By applying atomic force microscopy, surface force spectroscopy, circular dichroism, and in situ attenuated total reflection Fourier-transform infrared spectroscopy, structural changes of rSilC-silaffin upon its adsorption to polyelectrolyte surfaces prior to and during titania nanoparticle growth are revealed. It is demonstrated that the adhesion of rSilC-silaffin onto polyelectrolyte surfaces results in its reorganization from a random-coil conformation in solution into a mixed secondary structure with both random coil and β-sheet structures presented. Moreover, the protein forms a continuous molecularly thin layer with well-defined monodisperse nanodomains of lateral dimensions below 20 nm. It is also shown that rSilC embedded inside the polylelectrolyte matrix preserves its titania formation activity. It is suggested that the surface-mediated, bio-enabled synthesis of nanostructured materials might be useful to develop general procedures for controlled growth of inorganic nanomaterials on reactive organic surfaces, which opens new perspectives in the design of tailored, in situ grown, hybrid inorganic–organic nanomaterials.

1. Introduction

Recent years have seen a growing interest in the creation of nanometer-scale inorganic and hybrid materials using biological systems as catalysts, microreactors, and supporting templates.[1–9] The advantages of biomolecule-enabled syntheses of inorganic materials as compared with traditional chemical syntheses includes ambient conditions such as room temperature, aqueous environment, and neutral pH.[10] The use of biotemplates for the synthesis of inorganic nanoparticles also allows for precise control over particle shape, size distribution, and their spatial arrangement, as well as providing a means to their self-assembly and guided assembly, which is critical in the fields of nanofabrication, nanoelectronics, and catalysis.[11–16]

To date, a wide range of biomolecules has been exploited for the synthesis and assembly of inorganic microstructures and nanomaterials.[17–24] Among these materials, TiO_2 is of special importance because of its current and prospective applications as a photocatalyst, UV blocker, photochromic pigment, and an oxygen sensor, for lithium batteries and solar cells.[25] To date, bio-enabled titania synthesis has been successfully achieved in solution with the assistance of biomolecules, which include the protein silicatein, silaffins, lysozyme, peptides, and individual amino-acids.[20,26–31]

Besides the studies carried out directly in solution,[20,26,28–30] there is a growing interest in bio-assisted nanostructured titania formation directly on engineered substrates (inorganic, organic, biological, or microfabricated materials) using bio-enabled surfaces such as supports with tethered biomolecules or templates from organisms.[32,33] For instance, titania nanotubes were generated on bioengineered flagella of mesophilic bacteria.[32] Silk–titania nanocomposite films with uniformly dispersed 80 nm titania nanoparticles at ambient temperature have been generated using a sol–gel method.[34] Recently, 3D microstructures composed of titania and ferritin layers with complex architectures have been obtained by alternate binding and mineralization of Ti-binding peptides.[33]

In an alternative approach, titania–organic hybrid nanomaterials with controllable physical structure and properties were obtained by using chemical bath-deposited (CBD) coatings, self-assembled layers (SAMs), or flexible synthetic templates such as layer-by-layer (LbL) assembled polyelectrolytes.[35–37] The LbL fabrication technique involves assembly of organized polyelec-

[*] Prof. V. V. Tsukruk, Dr. E. Kharlampieva, S. Singamaneni
School of Materials Science and Engineering
Georgia Institute of Technology
Atlanta, GA 30332 (USA)
E-mail: vladimir@mse.gatech.edu
Dr. J. M. Slocik, Dr. R. R. Naik
Air Force Research Laboratory
Materials and Manufacturing Directorate
Wright-Patterson Air Force Base
Dayton, OH 45433 (USA)
Dr. N. Poulsen, Prof. N. Kröger
School of Chemistry and Biochemistry
Georgia Institute of Technology
Atlanta, GA 30332 (USA)

DOI: 10.1002/adfm.200801825

trolyte multilayers with preformed titania nanoparticles[38,39] or with a titania precursor, titanium(v) bis(ammonium lactato) dihydroxyide (TIBALDH), followed by thermal treatment for the formation of tubular titania nanotubes,[40] hollow titania nanoparticles,[41,42] or titania shells.[43] CBD[36] and SAM[37] methods involve adsorption of TiO_2 from colloid suspensions and subsequent annealing with the solid substrates at 60 or 80 °C, respectively. However, these methods result in the formation of thick (from >100 nm to 40 μm)[34,36] and rough films with uncontrollable microscopic agglomerates that range from hundreds of nanometers to several micrometers.[37,38] A recent study demonstrated that monodisperse TiO_2 structures can be synthesized within the LbL deposition of TIBALDH and a branched polyelectrolyte, polyethyleneimine (PEI), at room temperature.[35] PEI–TIBALDH films were constructed by spraying or dipping deposition and resulted in multilayers of 5 nm crystalline titania nanoparticles.[35]

In our previous work, we applied a biotemplated synthesis enabled by silaffin proteins to organize polyelectrolyte matrices to produce titania nanomaterials.[44] We showed that a recombinant silaffin, rSilC, which is capable of titania synthesis in solution,[24] remained active when deposited on a polyelectrolyte surface and mediated the formation of uniformly dispersed titania nanoparticles on solid or flexible templates.[44] In the present study, we focus on the mechanism of protein-enabled, surface-mediated titania nanoparticle synthesis on polyelectrolyte templates with particular focus on the protein secondary structure after adsorption on the polyelectrolytes and in the course of titania formation.

Although the TIBALDH precursor utilized here has already been used in several studies for titania deposition on surfaces at ambient conditions in the presence of polyelectrolytes[35] or biomolecules,[33,44] the mechanism of the surface-mediated formation of titania from TiBALDH has remained unclear. For silaffin-mediated titania synthesis in solution, it was suggested that the high density of amino groups in these proteins enables binding of TiBALDH molecules, facilitates the hydrolysis of this complex, and catalyzes the polycondensation of the resulting Ti^{IV}-oxo/hydoxo species. A similar mechanism was suggested for the surface-mediated synthesis of titania.[35,44] However, the secondary organization of the surface protein layer involved in titania formation at polyelectrolyte surfaces has not been addressed.

Therefore, the intention here is to investigate how biomolecule-induced mineralization of titania occurs on surfaces as compared with that in solution. Specifically, the following questions will be addressed: How does the distribution of the protein on the surface affect the size and distribution of titania nanoparticles? What happens to the protein secondary structure upon adsorption on to polyelectrolyte surfaces and after titania formation? What makes titania nanoparticles monodisperse when synthesized on surfaces? Finally, does rSilC preserve its titania formation activity when encapsulated *within* the polyelectrolyte matrix?

In seeking to answer these questions, atomic force microscopy (AFM), surface force spectroscopy (SFS), circular dichroism (CD), and in situ attenuated total reflection Fourier-transform infrared spectroscopy (ATR-FTIR) were utilized to elucidate the protein conformational changes upon rSilC adsorption onto tailored polyelectrolyte surfaces and in the course of titania formation.

2. Results and Discussion

A schematic representation of titania formation by surface-adsorbed rSilC is shown in Figure 1. To control silaffin protein adsorption and to direct nanoparticle growth and organization within the ultrathin polyelectrolyte–protein films, we used LbL films composed of alternating layers of poly(allylamine hydrochloride) (PAH) and poly(sodium 4-styrenesulfonate) (PSS) as polymeric ultrathin (below 20 nm) matrices with a bilayer thickness of 3 nm and a surface microroughness below 0.5 nm.[44] rSilC was deposited by spin-casting on top of the polyelectrolyte film or encapsulated into the polyelectrolyte matrix (Fig. 1). Exposure of the polyelectrolyte–rSilC films to TIBALDH results in formation of TiO_2 nanoparticles grown on the top or within the polymeric matrix (see Experimental Section for details).

Our previous findings showed that rSilC, when adsorbed on top of a $(PAH/PSS)_2$ matrix terminated with PSS, formed domains of 1.6 ± 0.7 nm in height, which contained about 15 protein molecules (Fig. 2A).[44] Exposure of the rSilC-containing polyelectrolyte surface to a TIBALDH solution resulted in the formation of individual TiO_2 nanoparticles with average diameters of 6.0 ± 1.5 nm and a protein shell of 1 nm, which were evenly distributed over the surface with no evidence of microscopic aggregates (Fig. 2B and C). We also found that the surface concentration of protein domains controlled the concentration of titania nanoparticles (Fig. 1S in the Supporting Information).

The difference in the overall titania nanostructures obtained by the surface-mediated approach suggested in our previous work as

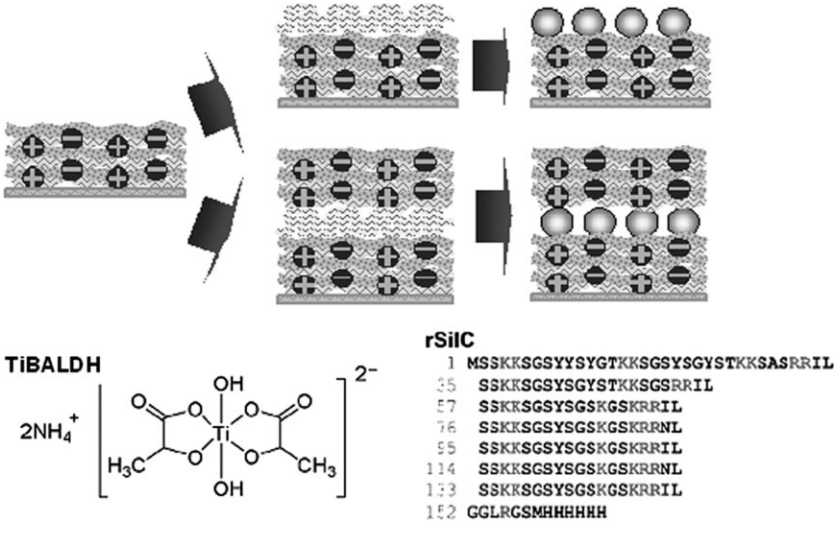

Figure 1. rSilC-mediated synthesis of titania nanoparticles on top of or within a polyelectrolyte matrix (top). Chemical structure of TiBALDH and amino acid sequence (one letter code) of rSilC (bottom).

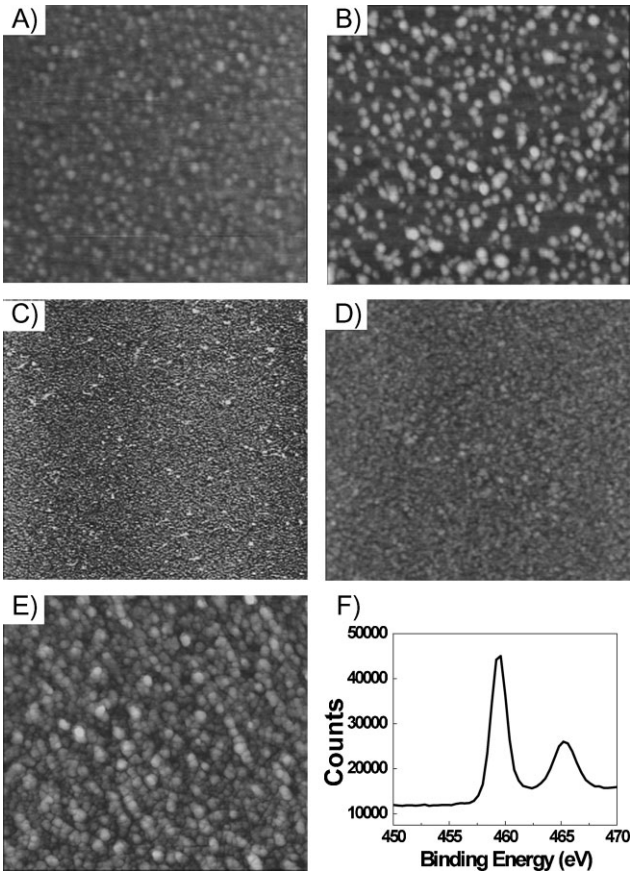

Figure 2. A–E) AFM images of a $(PAH/PSS)_2$–rSilC film (A) and a $(PAH/PSS)_2$–rSilC–$(PAH/PSS)_2$ film (D). The same films are shown after exposure to TiBALDH: $(PAH/PSS)_2$–rSilC (B,C), and $(PAH/PSS)_2$–rSilC–$(PAH/PSS)_2$ (E). The *Z*-scale is 10 nm. The scan size is $1 \times 1\ \mu m^2$ (A,B,D,E) and $10 \times 10\ \mu m^2$ (C). F) XPS spectrum of titania grown within a $(PAH/PSS)_2$–rSilC–$(PAH/PSS)_2$ film.

compared with the solution-based method is shown in Figure 3. The optical microscopy image of titania nanoparticles grown on an rSilC-containing polyelectrolyte matrix confirms the absence of large microscopic aggregates (Fig. 3A) which, however, are prevalent in the titania induced by rSilC in solution (Fig. 3B). Transmission electron microscopy (TEM) imaging demonstrated that isolated 4 nm particles are obtained by rSilC-mediated titania formation on surfaces (inset in Fig. 3A), while much larger TiO_2 particles that form microscopic aggregates from 100 nm to 50 μm

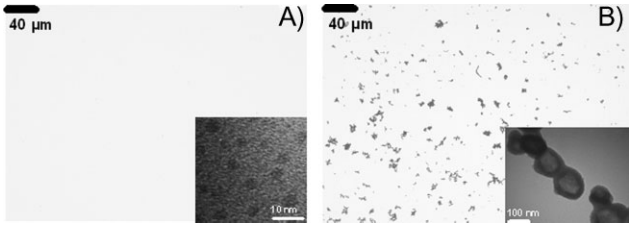

Figure 3. Optical microscopic images of rSilC-induced TiO_2 grown on a polyelectrolyte surface (A) and in solution (B). Insets: TEM of TiO_2 grown on the surface (A) and in solution (B).

were produced by rSilC-induced titania formation in solution (Fig. 3B).

To further analyze the distribution of protein domains on a polyelectrolyte surface, we employed SFS mapping. Figure 4 shows the adhesion map of the rSilC deposited on the surface of a $(PAH/PSS)_2$ film. One can observe a uniform adhesion over the $1 \times 1\ \mu m^2$ area with a unimodal distribution of the adhesive forces of the adsorbed protein despite the domain morphology visible in high-resolution AFM images (Fig. 2A). The silicon oxide surface of the AFM tip is moderately negatively charged, and in the case of a non-uniform distribution (i.e., only local domains without protein molecules in between domains) a bimodal distribution of the adhesion of the positively charged rSilC protein across the negatively charged PSS surface would be expected. Therefore, the unimodal distribution of tip–surface interactions suggests that the entire surface is covered with rSilC molecules. As the highest resolution of SFS achievable here (30 nm per pixel) is not sufficient to resolve the individual rSilC domains, the result indicates that the rSilC domains are surrounded by a molecular layer of rSilC molecules (see below for further discussion).

Next we investigated if rSilC remains active towards titania formation after being encapsulated within the polyelectrolyte matrix (Fig. 1). To achieve this, a polyelectrolyte film with a tethered layer of rSilC $(PAH/PSS)_2$–rSilC, was coated with two bilayers of PAH/PSS and then exposed to a TIBALDH solution for 7 days. Subsequent AFM analysis detected growth of titania nanoparticles as was evident from the increase in surface roughness from 0.4 nm to 1.2 nm after TIBALDH exposure (Fig. 2D and E). The presence of titania inside the LbL matrix was confirmed by angle-resolved X-ray photoelectron spectroscopy (XPS) showing the sharp Ti $2p_{3/2}$ peak located at 458.8 eV, which corresponds to the reference value of titania (Fig. 2F). According to the XPS depth profile, the ratio of Ti 2p to C 1s for embedded titania is nearly the same (1:11) as for titania grown on the surface when measured at 15°, 45°, and 80° take-off angles, which correspond to the top, middle, and bottom regions of the film, respectively (not shown). In contrast, XPS analysis did not detect titania in the absence of an rSilC layer in the films under identical conditions (data not shown). Thus, rSilC domains are able to initiate the formation of titania nanoparticles not only on top of a polyelectrolyte surface, but also in a confined environment. The results indicate that the surface-mediated approach of rSilC-induced titania formation is not limited to the top surface only, but can be applied for titania growth within an ultrathin LbL matrix.

2.1. rSilC Structure in Solutions and Surfaces Monitored by CD and ATR-FTIR

To investigate why biomolecule-induced mineralization of titania on surfaces differs from that in solutions in term of the resulting nano- and microstructures, we first studied how rSilC adsorption onto the polyelectrolyte surface affects the protein's secondary structure.

First, we conducted CD and FTIR measurements on a protein solution. A CD spectrum of rSilC in solution revealed a slight negative dip at 199 nm, which is characteristic for a random coil conformation[45,46] (Fig. 5A). FTIR spectroscopy was then applied

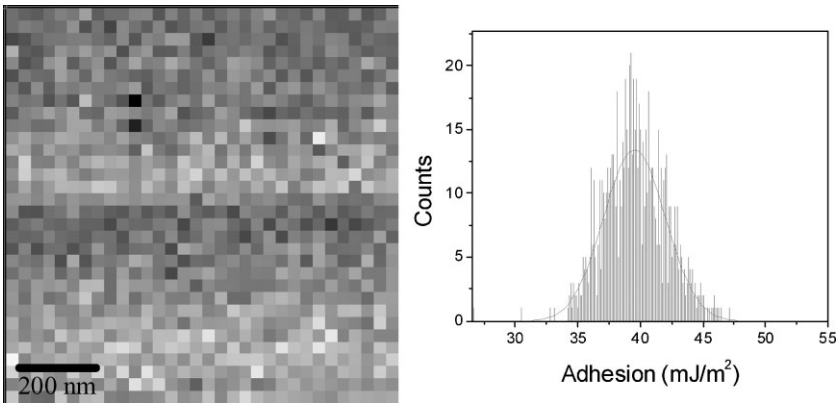

Figure 4. Force–volume measurements of a $(PAH/PSS)_2$–rSilC film with an adhesion map showing the smooth surface morphology and uniform adhesion. Histogram of the adhesion and the corresponding Gaussian fit showing the unimodal distribution.

as an independent technique that allows fine resolution of a protein's secondary structure.[40,47–49] The FTIR spectrum of rSilC in solution showed a characteristic amide I band (1600–1700 cm^{-1}), which is associated with C=O stretching vibrations in the protein backbone coupled to the N−H bending and C=N stretching modes (Fig. 5B).[47] In the spectrum obtained, the amide I band is centered at 1644 cm^{-1}, which is consistent with a random coil conformation for the proteins.[50,51] Thus, both spectroscopic techniques supported the random conformation of silaffin in a dilute solution.

In striking contrast, the rSilC conformation in spin-cast films appears to be very different. The CD spectrum reveals a predominant β-sheet conformation for rSilC deposited on either a PAH and PSS-terminated surface as indicated by strong positive and negative bands at 192 and 218 nm, respectively (Fig. 6A).[51,52] The β-sheet structure was also preserved in the rSilC layer that was retained on a PSS-tethered surface after dissolving the 'thick' cast film by incubation in H_2O for 1 h followed by intensive rinsing with H_2O (Fig. 6B).

In addition, ATR-FTIR spectra of a cast rSilC film before and after rinsing with H_2O also revealed significant reorganization of the secondary structure (Fig. 7). The 150 nm thick film was prepared by spin-casting a 1.5 mg mL^{-1} protein solution in D_2O on a surface of an ATR silicon crystal pre-coated with a two-bilayer PAH/PSS film, and then intensively rinsed with D_2O (Fig. 7A and B) to obtain a residual 3 nm film, as measured by ellipsometry. In fact, spectra for both protein films exhibited a strong peak at 1618 cm^{-1}, which is observed in the FTIR spectrum of the protein in solution (Fig. 5B). The peak is diagnostic of the presence of a β-sheet conformation (absorption at 1610–1625 cm^{-1}) thus confirms the CD spectroscopy results.[50,51,53,54]

To quantitatively analyze the secondary structure of the protein in solution and in a solid state, the complex peak in the FTIR spectra was deconvoluted using a curve-fitting procedure in accordance with literature data (Fig. 8).[47,55] As is known, amide I bands in this wavenumber range are usually unaffected by the exchange of H_2O to D_2O and can, therefore, be used for the conformational analysis of proteins.[56–58]

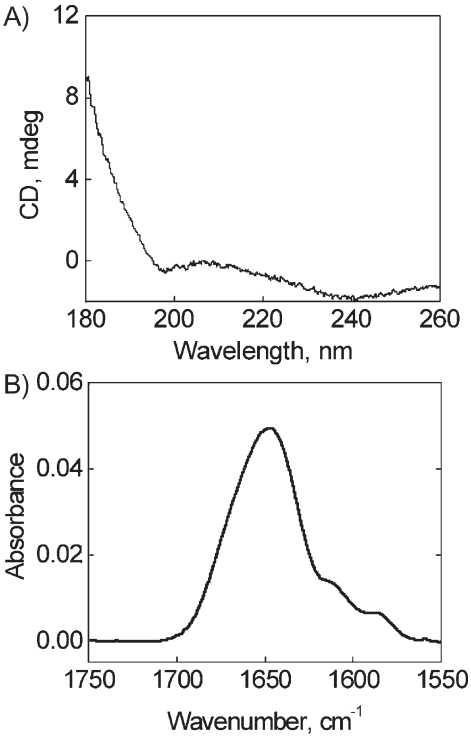

Figure 5. Representative CD (A) and ATR-FTIR (B) spectra of rSilC in D_2O solutions.

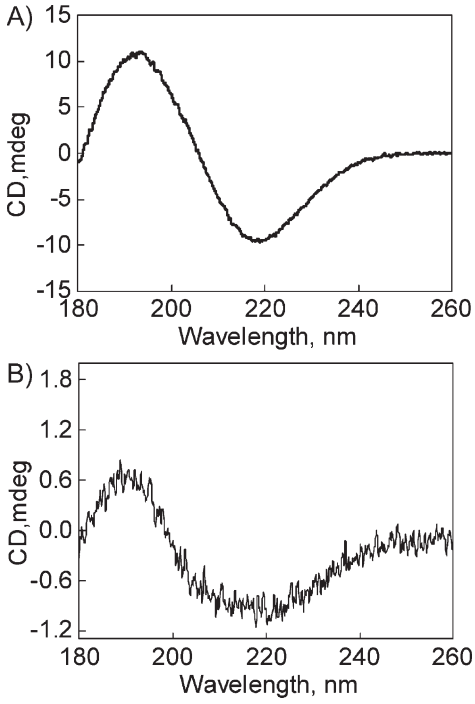

Figure 6. CD spectra of a rSilC film as cast (A) and rinsed with D_2O (B).

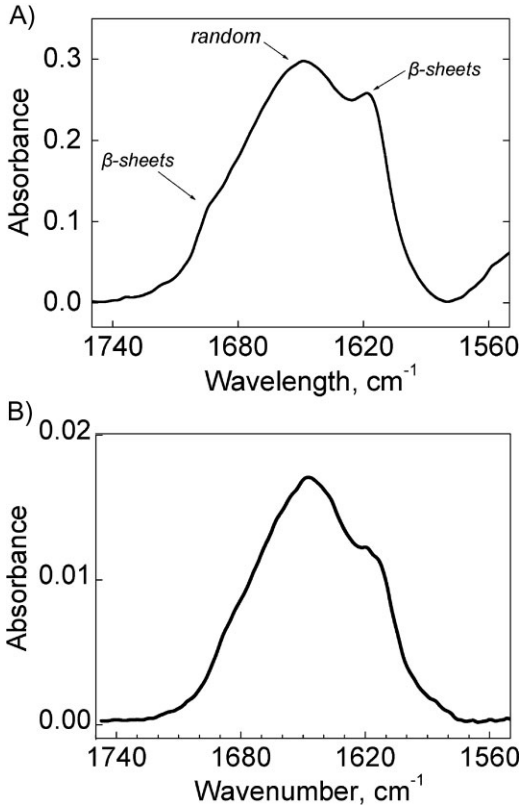

Figure 7. ATR-FTIR spectra of rSilC within an as-prepared cast film (A) and within a cast film after rinsing with D_2O (B).

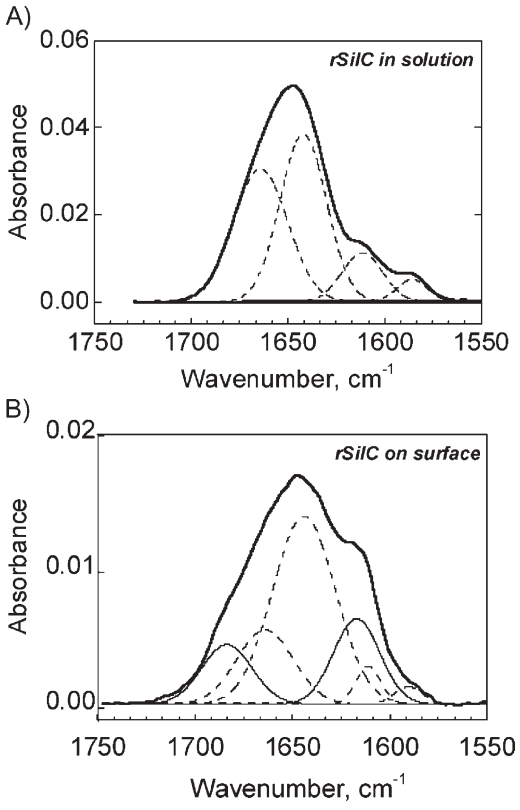

Figure 8. ATR-FTIR spectra deconvolution of rSilC films in a hydrated (A) and dry state (B). Peaks attributed to β-sheets (centered at 1683 and 1618 cm^{-1}) are shown with solid lines (B).

According to this approach, the amide I band obtained from rSilC in solution can be deconvoluted into two major peaks centered at 1664 and 1642 cm^{-1} (Fig. 8A). These two peaks are usually associated with unordered turns and a random coil, respectively.[50,51,59] In contrast, for the ultrathin film of rSilC on a polyelectrolyte surface, the peak deconvolution revealed two additional peaks centered at 1683 and 1618 cm^{-1}, which can be attributed to the presence of β-sheets in addition to random coils[51,54] (Fig. 8B). Integration of the band intensities suggests a 40% β-sheet content in the solid film. No evidence of α-helix structures (peaks in the 1655–1652 cm^{-1} region[47,59,60]) can be found in the spectra. The peaks at 1610 cm^{-1} in both spectra are likely a result of asymmetric stretch vibrations of arginine side groups. The spectra of both samples also show vibrational peaks in the amide II region (1500–1600 cm^{-1}), which are associated with N−H bending[47] and may be assigned to aromatic amino-acid groups (note: rSilC has a relatively high content of tyrosine).[57,61]

Altogether, CD and ATR-FTIR results clearly indicate that rSilC has a random coil conformation in solution, but acquires mixed (random coil and β-sheet) secondary structures when deposited on polyelectrolyte surfaces. The rSilC secondary structure appears to be the same in ultrathin (3 nm) films and cast (150 nm) films. Changes in protein conformation upon adsorption onto polyelectrolyte surfaces have been previously studied for globular proteins that exhibit an organized secondary structure in solution.[49,54,55,62–64] This has revealed that polyelectrolyte LbL multilayers can create a favorable environment for the incorporated proteins, which results in the preservation of their secondary structure and activities.[63,65,66] In some cases, however, the secondary structure of globular proteins were altered upon deposition on polyelectrolyte films and resulted in a decrease in α-helix content with an increase in β-sheet content. These alterations in the proteins' secondary structure resulted from 'asymmetric' interactions as a result of facing the electrostatic surface on one side and water on the other side of the film.[54]

Much less is known about the conformational transitions of proteins with random coil conformations when they form solid films on surfaces. One example is silk as a fibrous protein: it has a random-coil conformation in solution and retains this conformation in cast films as well as in electrospun fibers. However, upon treatment with organic solvents or when exposed to elevated temperature, the solid-state films and fibers of silk undergo a transition into a β-sheet conformation.[67–69] The other example involves poly(L-lysine) (PLL), which is known to adopt a random coil conformation at low and neutral pHs in solution (containing a maximum positive charge density), but then transforms into α-helices at basic pH values or into β-sheets upon heating or interaction with polyelectrolytes.[50,70] Similar to silk, when PLL is cast onto solid templates and dehydrated, its conformation changes from a random coil to a mixture of random coil and β-sheet conformations. The mechanism of such a transformation is not clearly understood. It was suggested that the proximity to a surface was a key factor in inducing these conformational

transformations.[53] Since partial dehydration of such films upon treatment with heat or polar solvents additionally increases the β-sheet content, the dehydration process was suggested to induce additional inter and intra-molecular binding through enhanced hydrophobic interactions followed by the formation of β-sheets.[71]

Like PLL, the rSilC protein utilized here is a highly polycationic molecule at physiological pH (pI = 11.8) because of its high lysine and arginine content[29] (Fig. 1). Therefore, it adopts a random coil conformation in solution as a result of electrostatic repulsion between the positively charged amino groups. It is worth noting that rSilC in a solid state undergoes conformational changes to adopt a partial β-sheet structure similarly to PLL. By analogy to previous findings with other proteins (see above), we suggest that both the proximity to a surface enriched with negatively charged groups and partial dehydration upon drying are responsible for the structural transformation of rSilC. At present it is unclear whether the experimentally observed structural reorganization of the rSilC molecules from random coil into β-sheet upon surface binding occurs predominantly within the protein domains or within molecular layers between the protein domains, or within both. Further studies will be needed to fully understand the reason for such conformational transitions of rSilC.

2.2. rSilC-Induced Mineralization of Titania

To further investigate how the rSilC secondary structure is affected by titania nanoparticle formation, CD spectroscopy was applied to study the structure of the pure protein in D_2O and the titania-associated protein (i.e., after mixing with TIBALDH in phosphate buffer at pH 7). It was found that both the pure protein and the titania-associated protein exhibit random coil conformations (Fig. 9A). CD spectroscopy of rSilC films before and after titania formation confirmed no changes in secondary structure of rSilC (Fig. 9B). Therefore, binding of TIBALDH followed by titania formation does not alter the global secondary structure of rSilC, whereby the β-sheet conformation of rSilC remained largely unchanged during titania formation.

As a result of our studies, a possible mechanism for rSilC-induced monodisperse titania nanoparticle formation on the polyelectrolyte surface can be suggested as illustrated in Figure 10. This model considers that protein deposition onto polyelectrolyte surfaces results in the formation of nanometer-scale rSilC domains that are evenly distributed over the surface and surrounded by a monolayer of rSilC molecules as is suggested by the results of the AFM and SFS studies. It is suggested that after exposure of the rSilC film to a precursor solution, anionic TIBALDH molecules are accumulated by cationic rSilC predominantly within the domains (Fig. 10).[44] Indeed, the fact that the surface coverage with titania nanoparticles correlates very well with the concentration of protein domains on the surface, supports this suggestion.[44]

It is suggested that the accumulation of the precursor continues until a certain limit governed by the charge balance with negatively charged TIBALDH molecules, which diffuse into the highly positively charged protein domains and eventually bind to the protein backbones. Such binding may result in amino-group catalyzed hydrolysis of the TIBALDH precursor followed by

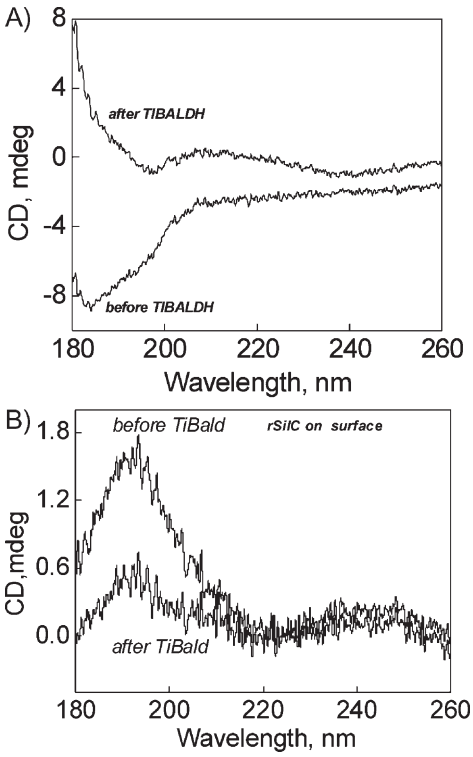

Figure 9. CD spectra of rSilC before and after titania formation in D_2O solutions (A) and on a PSS-tethered polyelectrolyte surface (B). $(PAH/PSS)_2$ layer was deposited on a quartz slide, and rSilC was subsequently bound to the polyelectrolyte surface.

growth of titania nanoparticles, similar to the mechanism suggested for rSilC-induced TiO_2 formation in solutions.[17,29] In addition, the discrete domains of rSilC aggregates prevent the further aggregation of nanoparticles, in contrast to microscopic aggregates of titania precipitates formed in solution. Note that the slow growth of titania on surfaces as compared with the immediate precipitation of titania from solution[17,29] may be attributed to the slow diffusion of TIBALDH molecules into the surface-confined protein domains. We speculate that titania nanoparticles are not formed in between the domains because of the lack of a sufficiently high charge accumulation as the positive charge of the rSilC monolayer is largely compensated by the negative charge of the PSS-tethered LbL surface.

We can estimate the feasibility of forming titania nanoparticles with a diameter 3.9 nm within a single protein domain with a lateral dimension of 20 nm (estimated from AFM images that account for the AFM tip dilation) by considering the charge balance

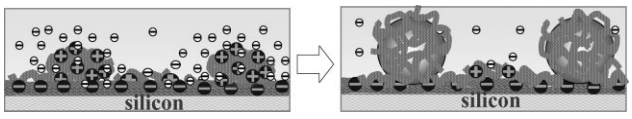

Figure 10. Schematic of the suggested mechanism for rSilC-induced titania formation on PSS-tethered polyelectrolyte surfaces. The minus signs (close to the silicon surface) represent the negative charges of the PSS residues, the small minus signs stand for TiBALDH molecules. The grey strings represent rSilC molecules and their associated positive charges (plus signs). The spheres on the right panel indicate titania nanoparticles.

within each protein domain and in the presence and absence of TIBALDH molecules. In fact, as can be estimated from domain dimensions and molecular volumes of protein chains, an average protein domain is composed of about 15 protein molecules.[44] Considering that each protein molecule possesses 45 positive charges,[29] the entire domain carries ~700 charges. Assuming that at least 100 charges are compensated by the negatively charged PSS surface with a surface charge density of 2–3 nm^2 per charge beneath the adsorbed protein, one can conclude that each domain carries ~600 positive charges available for binding of negatively charged $TIBALDH^{2-}$ molecules. Thus, assuming that TiBALDH diffusion into a protein domain stops after full charge compensation caused by precursor binding to all protein segments, we can estimate that about 300 TiO_2 species can be formed within each protein domain. The result agrees well with the estimation of a 3.9 nm titania nanoparticle (assuming a purely amorphous phase) being composed of ~300 TiO_2 or about 900 TiO_2 molecules (assuming a purely anatase phase).[72] Considering that Raman measurements suggest mixed anatase and amorphous phases,[44] we conclude that titania nanoparticles may be composed of a mixture of anatase and amorphous phases with some residual TiBALDH molecules.

3. Conclusion

In summary, we found that protein deposition onto PSS-terminated polyelectrolyte surfaces results in protein reorganization from a random-coil to a mixture of random-coil and β-sheet secondary structures. In addition, rSilC forms a dense and continuous layer of nanometer-scale domains evenly distributed over the polyelectrolyte surface. We further demonstrated that rSilC embedded inside a polyelectrolyte matrix preserved its titania formation activity, which may open new routes towards the design of hybrid inorganic–organic nanopatterned materials.

We believe that understanding the mechanism of biomolecule-induced mineralization on tailored charged surfaces as compared with that in solution will be useful to develop general procedures for controlled titania formation on surfaces and in bulk solutions. Moreover, the knowledge of the structural and compositional analysis of precursor-protein interactions presented here can be expanded to other reactive synthetic molecules or biomolecules to be adapted for a wide range of surface-mediated bio-enabled inorganic synthetic strategies.

4. Experimental

Materials: PAH ($M_w = 65\,000$), PSS ($M_w = 70\,000$), and TIBALDH were purchased from Aldrich. The recombinant silaffin rSilC (17 625 Da) was prepared as described previously [28]. Nanopure water with a resistivity of 18.2 MΩ cm was used in all experiments. D_2O with 99.9% isotope content was purchased from Cambridge Isotope Laboratories and was used as received. To control the pH and ionic strength, concentrated HCl and the inorganic salts NaCl, Na_2HPO_4, and NaH_2PO_4 (General Storage, pure grade) were used as received.

Multilayer Deposition and Titania Synthesis on Silicon Wafers: Multilayered films and protein depositions on silicon wafers were produced by a spin-assisted LbL (SA-LbL) method, which is a combination of spin coating and conventional LbL techniques [73]. Specifically, 30 μL of 1 mg mL^{-1} polyelectrolyte solutions were sequentially dropped onto silicon substrates, rotated for 20 s with a 5000 rpm rotation speed (Laurell Co.), and rinsed twice with H_2O between the deposition cycles. rSilC was then deposited from 1.5 mg mL^{-1} solutions on the surface of the polyelectrolyte films. Unbound protein was removed by extensive rinsing with H_2O. Formation of TiO_2 particles was achieved by exposure of the polyelectrolyte–rSilC film to 0.2 M TIBALDH solution in 0.05 M citrate-phosphate for 7 days at 24 °C in the dark, followed by extensive rinsing with H_2O.

Instrumentation: Protein deposition and mineralization on silicon wafers were monitored by AFM (Dimension 3000 microscope, Digital Instruments). AFM images were collected in the tapping mode with silicon tips with a spring constant of 50 N m^{-1} in accordance with usual procedures adapted in our laboratory [74]. AFM nanomechanical measurements of the rSilC layer (force–volume) were performed on the PSS surface tethered with rSilC by collecting 32×32 point arrays of force–distance curves [75,76]. The cantilever calibration, data processing, and evaluation of the adhesion distribution were performed by a usual approach using the Hertzian contact mechanic model [77]. In brief, an AFM tip with known shape (deconvoluted by scanning a gold-nanoparticle reference specimen) indents the surface with a probing frequency of 1 Hz. The indentation depth was limited to ~0.5 nm to avoid any plastic deformation, yet probe the adhesion between the AFM tip and the surface.

Ellipsometry measurements of layer thicknesses were performed by using a M2000U (Woolam) spectroscopic ellipsometer. The elemental composition was determined by averaging four spots (800 micrometer spot size) on each wafer by XPS performed on a Surface Instruments (SSI) M-probe instrument operated at a base pressure of 3×10^{-7} Pa using an operating voltage of 10 kV. TEM was performed with a JEOL 100CX-2 electron microscope at 100 kV. High resolution TEM (HRTEM) images were collected on a Phillips CM200 TEM Lab6 operating at 200 kV equipped with a Thermo Electron EDAX detector. TEM and HRTEM were performed on free-standing $(PAH/PSS)_{20}$–rSilC–TiO_2 films transferred to Cu grids.

CD measurements were performed on a Jasco J-815 CD spectrometer. Samples were scanned from 260 to 180 nm at 20 nm min^{-1}, averaged over four scans, and rotated at several different orientations to ensure sample homogeneity across the film. Samples were prepared on a quartz CD plate by casting 50 μL of a 1.5 mg mL^{-1} solution of rSilC in H_2O or D_2O and air drying.

ATR-FTIR measurements: ATR-FTIR spectra were collected using a Bruker FTIR spectrometer (Vertex 70) equipped with a narrow-band mercury cadmium telluride detector. The internal compartment of the FTIR spectrometer that contained the liquid cell was purged with dry nitrogen. The ATR surface was a rectangular trapezoidal Si crystal of dimensions 50 mm × 10 mm × 2 mm (Harrick Scientific) whose beam entrance and exit surfaces were cut at 45 degrees. Spectra were collected at 4 cm^{-1} resolution, and the number of averaged scans was 120. To obtain the absorbance spectra, each interferogram was divided by the corresponding background, measured for the same ATR cell with the same D_2O buffer solution. The bare ATR crystal was used as a background. To eliminate overlap of the IR spectra of polyacids and proteins in the 1700–1500 cm^{-1} region with the strong water band, D_2O was used as a solvent. Although the acidity was determined by deuterium rather than hydrogen ions, we nonetheless refer to it as pH.

Multilayer films of $(PSS/PAH)_n$ were deposited on a hydrophilic Si crystal in situ within the flow-through ATR-FTIR liquid cell obtained from Harrick Scientific. Multilayer deposition was performed using the procedure described elsewhere [47]. Briefly, 0.1 mg mL^{-1} solutions of PAH in 0.01 M buffer solution was allowed to adsorb onto the surface of the oxidized Si crystal at a pH 5 for 10 min, and after that the polymer solution was replaced by the buffer solution without polymer. A PSS layer was then deposited from a 0.1 mg mL^{-1} solution in the same buffer and the deposition cycle was repeated.

Protein was then adsorbed on the top of the film by spin-assisted deposition similar to that applied for silicon wafers. Specifically, the ATR Si crystal pre-coated with a two-bilayer PAH/PSS film was taken out of the liquid cell and set on a spin-coater. A D_2O solution of rSilC (1.5 mg mL^{-1}) was dropped on one side of the crystal and rotated until dried. The spectrum of the 'thick' cast film was performed in a dry flow-through cell by taking the dry clean Si crystal as a background. To obtain the spectrum of a 'thin' protein film, the unbound protein was removed by setting the crystal

back to the spin-coater and extensively rinsing with D_2O. The same result was obtained if H_2O was used instead D_2O. Film thicknesses were determined by ellipsometry.

Solution FTIR analysis was performed on a Nicolet Magna II-550 FT-IR spectrometer equipped with a liquid nitrogen-cooled MCT/A detector and a KBr beam splitter [78]. The mirror velocity was 2.53 cm s^{-1}, the spectroscopic resolution was 2 cm^{-1}, and 2000 mirror scans were accumulated. The sample (6 μL) was placed between two 19 mm CaF_2 windows (Harrick Scientific) using a 6 μm spacer. A Harrick temperature control cell and a recirculating water bath were used to control the temperature at 20 °C. The protein concentration was 10 mg mL^{-1}. To obtain the spectrum, a buffer spectrum was recorded, and this spectrum was subtracted.

The infrared absorption peaks were baseline corrected and integrated with Galactic Grams/32 software using curve fitting. The relative contribution of the spectra components were obtained by integration of the band areas. In the fitting procedure the wavenumbers, widths, and Gaussian band profiles were fixed, but peak intensities were varied for different spectra. For each protein layer a curve-fitting file with the fixed parameters was created and applied to all spectra for consistency.

Acknowledgements

This work was supported by funding provided by the Air Office of Scientific Research, Air Force Research Laboratory, National Science Foundation, and the Office of Naval Research. The authors acknowledge S. Bender and B. Barry (Georgia Institute of Technology) for solution FTIR measurements. Supporting Information is available online at Wiley InterScience or from the author.

Received: December 9, 2008
Published online: May 14, 2009

[1] L. Chunmei, D. Kaplan, *Curr. Opin. Solid. State. Mater. Sci.* **2003**, *7*, 265.
[2] S. Mann, *Biomineralization Principles and Concepts in Bioinorganic Materials Chemistry*, Oxford University Press, Inc., New York **2001**.
[3] J. Aizenberg, *Adv. Mater.* **2004**, *16*, 1295.
[4] G. Hodes, *Adv. Mater.* **2007**, *19*, 639.
[5] L. C. Palmer, Y. S. Velichko, M. Olvera De La Cruz, S. I. Stupp, *Phil. Trans. Math. Phys. Eng. Sci.* **2007**, *365*, 1417.
[6] N. Harris, J. Kohn, *Biomaterials Informatics*, John Wiley and Sons, Inc., New York **2007**.
[7] R. Naik, S. Stringer, G. Agarwal, S. Jones, M. Stone, *Nat. Mater.* **2002**, *1*, 169.
[8] K. Rajangam, H. A. Behanna, M. J. Hui, X. Han, J. F. Hulvat, J. W. Lomasney, S. I. Stupp, *Nano Lett.* **2006**, *6*, 2086.
[9] S. I. Stupp, J. J. J. M. Donners, L. S. Li, A. Mata, *MRS Bull.* **2005**, *30*, 864.
[10] J. Bill, *Adv. Sci. Technol.* **2006**, *45*, 643.
[11] V. Berry, S. Rangaswamy, R. F. Saraf, *Nano Lett.* **2004**, *4*, 939.
[12] E. Dujardin, S. Mann, *Adv. Mater.* **2002**, *14*, 775.
[13] S. Davis, E. Dujardin, S. Mann, *Curr. Opin. Solid. State. Mater. Sci.* **2003**, *7*, 273.
[14] S. Ludwigs, U. Steiner, A. N. Kulak, R. Lam, F. C. Meldrum, *Adv. Mater.* **2006**, *18*, 2270.
[15] K. Gorna, R. Munoz-Espi, F. Groehn, G. Wegner, *Macromol. Biosci.* **2007**, *7*, 163.
[16] J. Aizenberg, G. Hendler, *J. Mater. Chem.* **2004**, *14*, 2066.
[17] R. L. Brutchey, D. E. Morse, *Chem. Rev.* **2008**, *108*, 4915.
[18] M. Umetsu, M. Mizuta, K. Tsumoto, S. Ohara, S. Takami, H. Watanabe, I. Kumagai, T. Adschiri, *Adv. Mater.* **2005**, *17*, 2571.
[19] C. Thai, H. Dai, M. Sastry, M. Sarikaya, D. Schwartz, F. Baneyx, *Biotechnol. Bioeng.* **2004**, *87*, 129.
[20] S. Sewell, D. Wright, *Chem. Mater.* **2006**, *18*, 3108.
[21] N. Poulsen, N. Kröger, *J. Biol. Chem.* **2004**, *279*, 42993.
[22] Y. Liu, Z. Shen, L. Li, P. Sun, X. Zhou, B. Li, Q. Jin, D. Ding, T. Chen, *Micropor. Mesopor. Mater.* **2006**, *92*, 189.
[23] K. Sano, H. Sasaki, K. Shiba, *Langmuir* **2005**, *21*, 3090.
[24] G. Ahmad, M. Dickerson, B. Church, Y. Cai, S. Jones, R. Naik, J. King, C. Summers, N. Kröger, K. Sandhage, *Adv. Mater.* **2006**, *18*, 1759.
[25] D. Bavykin, J. Friedrich, F. Walsh, *Adv. Mater.* **2006**, *18*, 2807.
[26] O. Durupthy, J. Bill, F. Aldinger, *Cryst. Growth. Des.* **2007**, *7*, 2696.
[27] J. L. Sumerel, W. Yang, D. Kisailus, J. C. Weaver, J. H. Choi, D. E. Morse, *Chem. Mater.* **2003**, *15*, 4804.
[28] H. R. Luckarift, M. B. Dickerson, K. H. Sandhage, J. C. Spain, *Small* **2006**, *2*, 640.
[29] N. Kröger, M. B. Dickerson, G. Ahmad, Y. Cai, M. S. Haluska, K. H. Sandhage, N. Poulsen, V. C. Sheppard, *Angew. Chem.* **2006**, *45*, 7239.
[30] M. J. Pender, L. A. Sowards, J. D. Hartgerink, M. O. Stone, R. Naik, *Nano Lett.* **2006**, *6*, 40.
[31] M. B. Dickerson, S. E. Jones, Y. Cai, G. Ahmad, R. R. Naik, N. Kröger, K. H. Sandhage, *Chem. Mater.* **2007**, *20*, 1578.
[32] M. T. Kumara, M. Subra, B. Tripp, *J. Nanosci. Nanotechnol.* **2007**, *7*, 2260.
[33] K. Sano, S. Yoshii, I. Yamashita, K. Shiba, *Nano Lett.* **2007**, *7*, 3200.
[34] X. X. Feng, L. L. Zhang, J. Y. Chen, Y. H. Guo, H. P. Zhang, C. I. Jia, *Int. J. Biol. Macromol.* **2007**, *40*, 105.
[35] N. Laugel, J. Hemmerlé, N. Ladhari, Y. Arntz, E. Gonthier, Y. Haikel, J. C. Voegel, P. Schaaf, V. Ball, *J. Colloid Interface Sci.* **2008**, *324*, 127.
[36] Z. Burghard, A. Tucic, L. P. H. Jeurgens, R. C. Hoffmann, J. Bill, F. Aldinger, *Adv. Mater.* **2007**, *19*, 970.
[37] T. P. Niesen, J. Bill, F. Aldinger, *Chem. Mater.* **2001**, *13*, 1552.
[38] R. Kniprath, S. Duhm, H. Glowatzki, N. Koch, S. Rogaschewski, J. P. Rabe, S. Kirstein, *Langmuir* **2007**, *23*, 9860.
[39] T. J. Dawidczyk, M. D. Walton, W. S. Jang, J. C. Grunlan, *Langmuir* **2008**, *24*, 8314.
[40] A. Yu, G. M. Lu, J. Drennan, I. Gentle, *Adv. Funct. Mater.* **2007**, *17*, 2600.
[41] F. Caruso, X. Shi, R. Caruso, A. Susha, *Adv. Mater.* **2001**, *13*, 740.
[42] K. Nelson, Y. Deng, *Nanotechnology* **2006**, *17*, 3219.
[43] K. S. Mayya, D. I. Gittins, F. Caruso, *Chem. Mater.* **2001**, *13*, 3833.
[44] E. Kharlampieva, T. Tsukruk, J. M. Slocik, H. Ko, N. Poulsen, R. R. Naik, N. Kröger, V. V. Tsukruk, *Adv. Mater.* **2008**, *20*, 3274.
[45] S. V. Patwardhan, R. Maheshwari, N. Mukherjee, K. L. Kiick, S. J. Clarson, *Biomacromolecules* **2006**, *7*, 491.
[46] C. Dicko, D. Knoght, J. M. Kenney, F. Vollrath, *Biomacromolecules* **2004**, *5*, 2105.
[47] V. Izumrudov, E. Kharlampieva, S. A. Sukhishvili, *Biomacromolecules* **2005**, *6*, 1782.
[48] C. Gergely, S. Bahi, B. Szalontai, H. Flores, P. Schaaf, J. C. Voegel, F. J. C. Cuisiner, *Langmuir* **2004**, *20*, 5575.
[49] M. Malmsten, *Biopolymers at Interfaces*, CRC Press, New York **2003**.
[50] M. Jackson, P. I. Haris, D. Chapman, *Biochim. Biophys. Acta* **1989**, *998*, 75.
[51] C. Dicko, D. Knoght, J. M. Kenney, F. Vollrath, *Biomacromolecules* **2004**, *5*, 2105.
[52] S. V. Patwardhan, R. Maheshwari, N. Mukherjee, K. L. Kiick, S. J. Clarson, *Biomacromolecules* **2006**, *7*, 491.
[53] J. Safar, P. Roller, G. C. Ruben, D. C. Gajdusek, C. J. Gibbs, *Bopolymers* **1993**, *33*, 1461.
[54] P. Schwinte, V. Ball, B. Szalontai, Y. Haikel, J.-C. Voegel, P. Schaaf, *Biomacromolecules* **2002**, *3*, 1135.
[55] L. Szyk, P. Schwinte, J. C. Voegel, P. Schaaf, B. Tinland, *J. Phys. Chem. B* **2002**, *106*, 6055.
[56] P. Wong, K. Heremans, *Biochim. Biophys. Acta* **1988**, *956*, 1.
[57] F. Wasacz, J. Olinger, R. Jakobsen, *Biochemistry* **1987**, *26*, 1464.
[58] R. Philp, D. McIver, P. Wong, *Biochim. Biophys. Acta* **1990**, *1021*, 91.
[59] A. Bentaleb, A. Abele, Y. Haikel, P. Schaaf, J. C. Voegel, *Langmuir* **1998**, *14*, 6493.
[60] N. Kossovsky, A. Nguyen, K. Sukiassians, A. Festekjian, A. Gelman, E. Sponsler, *J. Colloid Interface Sci.* **1994**, *166*, 350.
[61] L. Boulkanz, N. Balcar, M.-H. Baron, *Appl. Spectrosc.* **1995**, *49*, 1737.

[62] V. Ball, M. Winterhalter, P. Schwinte, Ph. Lavalle, J. C. Voegel, P. Schaaf, *J. Phys. Chem. B* **2002**, *106*, 2357.
[63] F. Caruso, D. N. Furlong, K. Ariga, I. Ichinose, T. Kunitake, *Langmuir* **1998**, *14*, 4559.
[64] S. A. Sukhishvili, S. Granick, *J. Chem. Phys.* **1999**, *110*, 20.
[65] K. Ariga, T. Kunitake, in *Protein Architecture, Interfacing Molecular Assemblies and Immobilization Biotechnology* (Eds: Y. Lvov, H. Möhwald), Marcel Dekker, New York **2000**, p. 169.
[66] M. Müller, T. Rieser, P. L. Dubin, K. Lunkwitz, *Macromol. Rapid Commun.* **2001**, *22*, 390.
[67] M. E. Rousseau, L. Beaulieu, T. Lefèvre, J. Paradis, T. Asakura, M. Pèzolet, *Biomacromolecules* **2006**, *7*, 2512.
[68] B. W. Hu, P. Zhou, I. Noda, Q. X. Ruan, *J. Phys. Chem. B* **2006**, *110*, 18 046.
[69] X. H. Zong, P. Zhou, Z.-Z. Shao, S.-M. Chen, X. Chen, B.-W. Hu, F. Deng, W. H. Yao, *Biochemistry* **2004**, *43*, 11 932.
[70] F. Boulmedais, P. Schwinte, C. Gergely, J. C. Voegel, P. Schaaf, *Langmuir* **2002**, *18*, 4523.
[71] J. G. Hardy, L. M. Römer, T. H. Scheibel, *Polymer* **2008**, *49*, 4309.
[72] To calculate the amount of titania molecules in anatase titania we used 80 g mol^{-1} and 3.84 g cm^{-3} as the titania molecular weight and density, respectively. For amorphous titania, the molecular weight of 168 g mol^{-1} and density of 1.9 g cm^{-3} for titania were taken. The molecular weight and density of TiBALDH are of 294 g mol^{-1} and 1.22 g cm^{-3}, respectively.
[73] C. Jiang, S. Markutsya, V. V. Tsukruk, *Adv. Mater.* **2004**, *16*, 157.
[74] V. V. Tsukruk, D. H. Reneker, *Polymer* **1995**, *36*, 1791.
[75] A. Kovalev, H. Shulha, M. Lemieux, N. Myshkin, V. V. Tsukruk, *J. Mater. Res.* **2004**, *19*, 716.
[76] H. Shulha, A. Kovalev, N. Myshkin, V. V. Tsukruk, *Eur. Polym. J.* **2004**, *40*, 949.
[77] V. V. Gorbunov, N. Fuchigami, J. L. Hazel, V. V. Tsukruk, *Langmuir* **1999**, *15*, 8340.
[78] R. S. Hutchison, S. D. Betts, C. F. Yocum, B. A. Barry, *Biochemistry* **1998**, *37*, 5643.